J. Fluid Mech. (1970), *vol.* 42, *part* 4, *pp.* 733–754
Printed in Great Britain

Laboratory studies of the velocity field over deep-water waves

By ROBERT H. STEWART

Scripps Institution of Oceanography
University of California, San Diego

(Received 11 August 1969 and in revised form 18 February 1970)

The mean-velocity field over monochromatic, 1·96 Hz, deep-water waves was measured by means of hot-wire anemometers for a range of wind speeds (relative to wave speed) of 0·4 to 3·0. The mean-velocity profile, over waves 0·64 cm in amplitude, was the same as that over a rough plate; that is, the mean velocity varied as the logarithm of the height above the mean-water level, except very close to the water, where the effect of the viscous sublayer became important. The wave-induced perturbation-velocity field and its associated Reynolds stresses were also measured and compared with numerical solutions of various linear equations governing shearing flow over a wavy boundary. The comparison showed that the measured velocity field was not well predicted by these theories.

1. Introduction

In order to understand how water waves grow, it is necessary first to understand the structure of the airflow over them. Early workers measured the mean-velocity profile as a function of height and found it to vary linearly with the logarithm of the height above the waves to a first approximation. This profile was used by Miles (1957, 1959), together with the inviscid Orr–Sommerfeld equation, to calculate the growth of water waves on the hypothesis that the wave-induced perturbations in the turbulent Reynolds stresses are negligible (inviscid quasi-laminar model). His results indicate that, for typical flows, the wave-induced Reynolds stresses have a step discontinuity in the region where the wind velocity equals the wave velocity, are constant below this region, and that the momentum is transferred to the wave predominately by normal stresses. Stewart (1961) estimated that this extraction of momentum from the mean flow should be large enough to significantly affect the mean-velocity profile, and the profile over water waves should differ from that over a roughened plate, especially in the lower regions; however, Miles (1965) disagreed and estimated that the effect should be small.

Recent measurements of velocity profiles have not resolved this disagreement. Laboratory measurements generally gave logarithmic profiles (Hidy & Plate 1966, Wu 1968), but not always (Shemdin & Hsu 1966, 1967; Shemdin 1967). The latter authors present some evidence that the profile over a crest of a wave differs from that over a trough. Field measurements, being much less accurate,

appear to be even more contradictory (Seeholzt 1968, Takeda 1963). Although most of the deviations from the logarithmic profiles were small, they could significantly effect the theory for the growth of water waves. Indeed, recent measurements of the growth of waves (Snyder & Cox 1966, Barnett & Wilkerson 1967, Shemdin & Hsu 1966, Bole & Hsu 1969) suggest that the inviscid quasi-laminar theory significantly underestimates their growth. In addition, recent measurements of fluctuations in the air over waves have also produced conflicting results. Measurements at British Columbia, in relatively shallow water, showed no wave-induced fluctuations in the air velocities, thus suggesting that the wave-induced flow calculated from linear theory may be wrong (Stewart 1967, Weiler & Burling 1967). However, measurement over waves in deeper water in the Atlantic suggest that waves do induce measurable fluctuations in the air (Seeholtz 1968).

In order to clarify the mechanism for the generation of waves, and to resolve part of the disagreement among previous measurements, this paper attempts to provide accurate measurements of the wave-induced flow over a simple, progressive, water wave in a laboratory wind tunnel, together with accurate, mean-velocity profiles. In comparing these measurements with theory, numerical solutions to the Orr–Sommerfeld equation were needed, and were kindly computed by Davis. The computation of these solutions motivated Davis to consider further the linear theory, and, ultimately, to new theoretical ideas, which are presented in Davis (1970). To facilitate the comparison of theory with data, we use the same notation as Davis. Furthermore, all data, except where noted, were non-dimensionalized by u_* and u_*/ν, where u_* is a friction velocity defined in § 4, and ν is the kinematic viscosity of air.

2. Equipment

The wind–water tunnel

The wind–water tunnel (figure 1) was an open return type, 57 cm wide by 59 cm high, 590 cm long, containing 21 cm of water in the bottom. The tunnel was equipped with a variable speed fan at the downwind end, a wave-maker at the upwind end, and beaches at both ends. An electrostatic filter was placed at the entrance to eliminate dust contamination of the hot-wire anemometers. The turbulence level, about 1 %, was considered sufficiently low for the intended experiment. The boundary layers were about 8 cm thick at the test section, and the flow was essentially constant throughout the central core. The range of wind speeds used was 56 to 227 cm/sec.

The wave-maker consisted of a submerged flat plate, hinged at the bottom, and was driven at variable frequency and amplitude. Considerable difficulty was encountered in getting the waves to travel down the tunnel as straight-crested waves, because waves whose wavelength was less than twice the width of the tunnel tended to become short crested as they travelled down the tunnel; the shorter the wavelength the faster this occurred. However, for wave frequencies below 2 Hz, the waves were reasonably two-dimensional, their amplitude varying about 20 % across the width of the tunnel; and therefore all data were collected

with 1·96 Hz waves. These waves have a wavelength of 40·8cm, a wave-number of 0·155 cm^{-1}, and a phase velocity of 79·6 cm/sec, assuming the wave is in deep water. This assumption introduces little error, since the bottom changes these values by only 0·3 %. The instruments were located 396 cm from the entrance and 274 cm from the wave-maker (6·7 wavelengths).

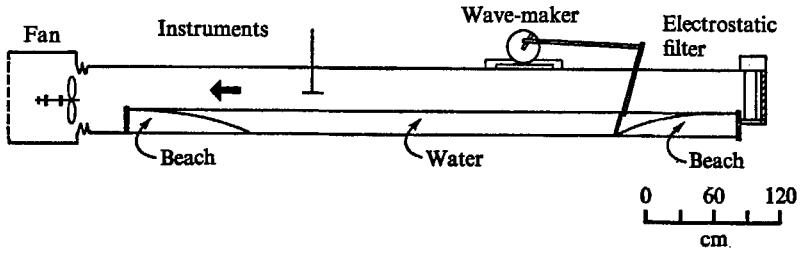

FIGURE 1. Schematic side view, wind–water tunnel.

Instrumentation

The water-surface elevation was measured by a resistance wave probe whose output varied linearly with depth of submergence. The air velocities were measured by a modified Shapiro and Edwards constant current hot-wire anemometer using two hot wires in an × configuration, the modification being that power was supplied externally by Harrison power supplies, and the amplification of the hot-wire signals was by Dymec amplifiers.

The hot wires were of 6·3 micron diameter platinum wire 0·27 cm long. They were mounted in a special probe that could rotate exactly 180° about an axis, precisely horizontal, which was aligned parallel to the tunnel axis. The axis of rotation passed midway between the two wires, so the rotation has the effect that one hot wire occupies the same position after rotation that the other occupied before rotation. The wires were operated in either of two fixed positions, rotated or non-rotated.

The d.c. voltage from the hot wires was largely removed by subtracting a known d.c. voltage from the hot-wire voltage; the remaining signal was amplified by a factor of 100. The two hot-wire voltages and the wave-recorder voltage were each sampled sequentially once every 48 ms, converted to a 12-bit binary number, and recorded on magnetic tape. Because the Nyquist frequency of the digital time series obtained from each signal was 10·42 Hz, the signals were filtered by 4-pole, multiple-feedback, low-pass filters to remove frequencies above 10 Hz before digitization.

3. Experimental method

General

The data were collected over a period of several months; but, to as close a degree as possible, all data were recorded under essentially the same conditions. The same hot wires were used throughout, and with the same current. All data were

recorded at night so that the room temperature remained constant within $\pm 0{\cdot}2\,^{\circ}\mathrm{C}$, although the temperature could vary $\pm 2\,^{\circ}\mathrm{C}$ from night to night. The data in each channel were sampled 4096 times, which represents a time of 196 sec or 386 wave periods. Two different sets of 4096 samples of data (representing 772 wave periods) were used to obtain each datum reported in this paper, thus ensuring statistically significant results.

Calibration

The hot wires were always calibrated *in situ* immediately prior to collecting data. Initially, the calibration was performed using a correlation between the vortex shedding frequency of a circular cylinder and the mean wind proposed by Roshko (1955) in the form

$$\frac{nd^2}{\nu} = 0{\cdot}212\frac{Ud}{\nu} - 2{\cdot}7, \tag{3.1}$$

where n = vortex shedding frequency, d = diameter of the cylinder, and ν = kinematic viscosity of air. For $d = 0{\cdot}635$ cm, $\nu = 0{\cdot}158$ cm^2/sec, and $70 < U < 250$ cm/sec, the Reynolds number, $R = Ud/\nu$, is in the range $280 < R < 1000$. For this range of R, the shed vortices have a well-defined frequency, but are turbulent, so the effects of the tunnel turbulence on the shedding frequency should be minimized. This initial calibration confirmed an accurate correlation between fan rev/min and mean-wind speed; consequently this was used to calibrate the anemometers. The wires were calibrated in both the rotated and the non-rotated position to eliminate any effect produced by the mean flow being at a slight angle to the tunnel axis.

The relative error in the calibration of the anemometers, as estimated from the variance in the measurement of n and the repeatability of the relationship between fan rev/min and the mean wind, was about $\pm 1{\cdot}5$ %. The absolute error of the calibration is difficult to assess, and depends essentially on the accuracy of (3.1). For a low-turbulence tunnel, Roshko's data indicates this equation is accurate to ± 2 %, but the effect of tunnel turbulence is unknown and may increase these estimates of error.

Analysis of data

The signals from the anemometers were analyzed assuming a linear response to small velocity fluctuations. The accuracy of this method was assessed by analyzing a portion of the data using both the non-linear and the linear hot-wire response function. A comparison of the results showed that the linear analysis underestimated the mean velocity, but never by more than $1{\cdot}5$ %. The values from the linear analysis of the fluctuating part of the velocity were within 7 % in amplitude and 3° in phase of the values from the non-linear analysis.

Accuracy

The errors in the velocity measurements fall into two classes. The first includes the effects of the inaccuracy of the electronic measurements, the temperature dependence of the hot-wires, the inaccuracy of the calibrations, and the drift of

the hot-wire calibration coefficients due to dust collecting on the wires; this class limits the accuracy of each velocity datum. The second includes errors due to the velocity fluctuations in the free stream and in the boundary layer; this class limits the precision of the measurements of the mean and perturbation velocity fields. A detailed discussion of both classes of errors is given in Stewart (1969). We present here a brief summary of the relative magnitudes of the first class, and defer until later a discussion of the second.

The electronics probably contributed an inaccuracy of $\pm 0{\cdot}1$ % to the measurements of the mean velocity, U, and ± 1 % to the measurements of the fluctuating velocities, $\mathbf{u}'$. The temperature changes of $\pm 0{\cdot}2$ °C contributed an inaccuracy of ± 1 % to U, while temperature fluctuations contributed an inaccuracy of ± 1 % to $\mathbf{u}'$. The change in U due to temperature was very slow, and its principal effect was to change the velocity profiles slightly. The drift of the calibration coefficients of the hot wires was negligible. The total drift after more than 50 hours of operation was less than the experimental inaccuracy of the measurement. This low drift was the result of the very high efficiency of the electrostatic filter at the low wind speeds used. Thus the values of the mean velocity are probably accurate to within ± 3 % on an absolute scale, and within $\pm 1{\cdot}5$ % on a relative scale.

In addition, there was an error in resolving the velocity components. Preliminary measurements, with a fixed $\times$ probe, indicated that the horizontal component of the velocity fluctuations at the wave frequency, $\mathscr{U}$, tended to be much larger than the vertical component, $\mathscr{W}$. Therefore a rotating probe was constructed so that if part of the measured $\mathscr{W}$ were due to $\mathscr{U}$, as a result of geometrical errors in resolving the velocity components, then rotating the probe about a horizontal axis would reduce this error. Measurements with the rotating probe, using the non-linear response function of the hot-wire, showed that over a wide range of velocities only about 1 % of U appears as a mean vertical velocity. This implies the fluctuating velocities are also resolvable to this accuracy.

4. Mean boundary-layer velocity measurements

The mean-velocity profile was measured for a number of free-stream velocities for air blowing over a smooth water surface in the absence of waves (although there were a few small ripples), and over smooth, 0·64 cm amplitude, sinusoidal waves. The former measurements were performed to obtain profiles that would be directly comparable to profiles measured over a smooth flat plate by other workers. Since the profile over a smooth water surface should be quantitatively similar to that over a smooth flat plate, except for the effects of a small surface current, this should provide an estimate of the accuracy of the measurements.

The measurements were made using the linear analysis. The mean voltages across the hot wires were converted to mean velocities; and the four mean velocities, obtained from the two wires operating in the rotated and non-rotated position at each elevation, were averaged together to obtain one point in the velocity profile.

The dimensional mean velocity, U^+, was plotted as a function of the logarithm of the dimensional height, z^+, for each free-stream velocity, U_∞. In general, the

velocity profile was linear on this plot, except at the lowest levels, and straight lines were drawn through the data for each profile. The slopes of these lines were used to define a friction velocity

$$u_* = k_0 \frac{dU^+}{d\ln z^+}, \tag{4.1}$$

assuming von Kármán's constant, k_0, was 0·4. The data were put into non-dimensional form using u_* and are plotted in figure 2. The symbols used in this figure, together with their associated free-stream and friction velocities, are given in table 1. The lines through the data in figure 2 were calculated from

$$U = 1/k_0 \ln(1+k_0 z) + A[1-(1+z/\delta)\exp(-z/\delta)] + B(z/\gamma)^2 \exp(-z/\gamma), \tag{4.2}$$

where

$$A = C_1 - 1/k_0 \ln k_0, \tag{4.3}$$

$$B = k_0 \gamma^2/2 - A\gamma^2/(2\delta^2). \tag{4.4}$$

The latter equation results from requiring $d^2U/dz^2 = 0$ at $z = 0$. The free parameters for the line through the data for flow over a smooth water surface are $C_1 = 7{\cdot}2$, $\delta = 4{\cdot}8$, and $\gamma = 1{\cdot}6$. The three different profiles through the data for flow over waves used $C_1 = 3{\cdot}7$ and the indicated values of δ and γ. No physical significance should be attached to (4.2), it is used only to provide a convenient functional relationship between the U and z data what will be useful in the linear perturbation analysis. Note that when $z > 60$ this equation reduces to the 'law of the wall'

$$U = 1/k_0 \ln z + C_1. \tag{4.5}$$

Before proceeding to a discussion of the mean-velocity measurements, we should consider the precision of these measurements since the flow through the tunnel was not steady, and repeated velocity measurements showed some variation. This variation was reduced to about 1 % of the nominal value of the mean velocity by the averaging together of the two 196 second segments of velocity data. Thus the precision and relative accuracy of the data were about equal. Nevertheless, there is one set of data points (no waves, $U_\infty = 56$ cm/sec) that seem to belie this estimate of accuracy. These data represent the lowest velocities measured in the tunnel, the velocity extending down to 24 cm/sec, and the accuracy of the hot-wire anemometers is questionable at these wind speeds. In addition, only the top four points in the profile were used to determine u_*, consequently u_* may be in error.

In comparing our data to previous work, we consider first the flow over a smooth water surface. Qualitatively, figure 2 agrees with a similar figure in Hinze (1959, page 478); that is, there exists a 'law of the wall' for $z > 30$ that blends into a viscous sublayer for $z < 30$. This effect of the viscous sublayer adequately explains why the data in the dimensional plots were not logarithmic in the lower regions. For a more detailed, quantitative verification of the data, we compare it with Coles's (1954) compilation of data for flow over a smooth plate. Since this compilation is for 'law of the wall' data, this comparison must be with u_* and C_1, the two parameters which characterize this correlation between U and z. Now, because u_* was used to reduce the data to non-dimensional form, figure 2 essentially determines the roughness coefficient C_1. Coles's figure 5 indicates C_1

[his $\phi(0)$] is a function of the momentum Reynolds number, R_θ, based on the momentum thickness of the boundary layer. Consequently, R_θ was estimated from (4.5) and was about 500; and C_1 should be about 6·2. This value is considerably smaller than our value of 7·2; however, if we account for the effects of a surface current, u_s, the agreement is better. To do this, let $u_s = C_2 u_*$, then $C_1 = 7{\cdot}2 - C_2$. We can estimate C_2 from Keulegan's (1951) or Baines & Knapp's

	No waves		Waves	
U_∞ (cm/sec)	u_* (cm/sec)	symbols used on figure 2	u_* (cm/sec)	symbols used on figure 2
227	10·10	○	11·68	○
193	8·70	□	—	—
155	7·25	▲	8·33	□ ▷
120	5·75	▷	6·71	▲
102	4·85	■ ●	5·76	●
95	—	—	5·49	■
86	4·13	▽	5·09	▽
56	2·92	◇	3·36	◇

TABLE 1. Summary of mean flow parameters

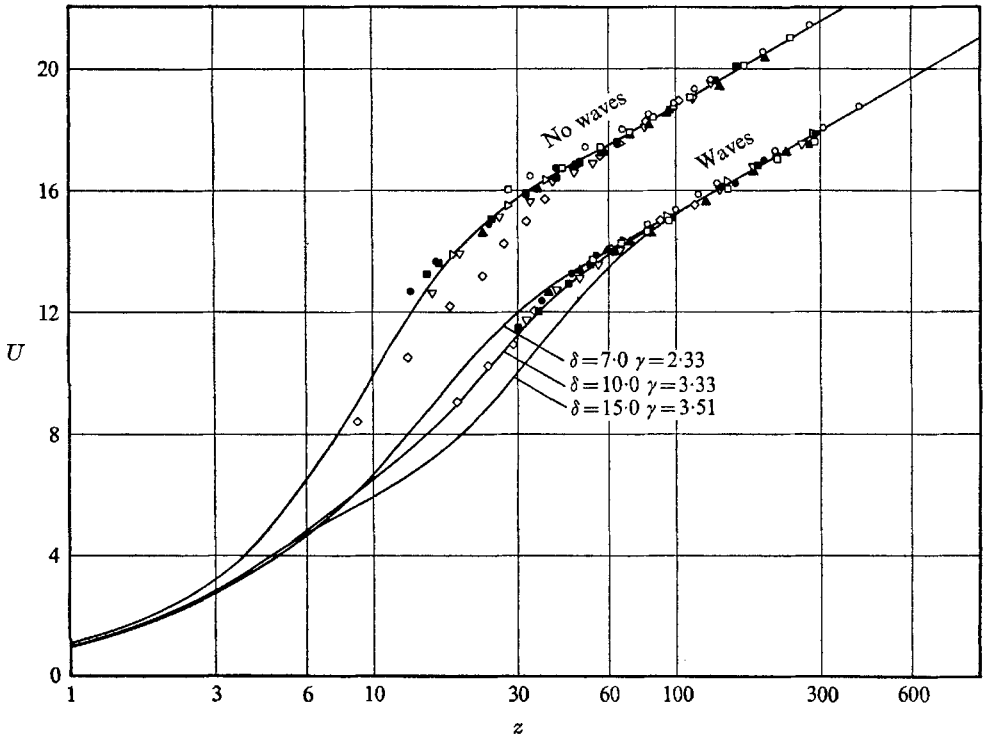

FIGURE 2. Mean wind velocity *vs.* height. The data symbols are identified in table 1; —, calculated from (4.2).

(1965) data, and can reasonably take it to be 0·6; therefore $C_1 = 6{\cdot}6$. Considering the scatter in C_2 and in Coles's value of C_1, our value of C_1 is not inconsistent with previous determinations of its value.

It remains to determine whether the measured values of u_*, for flow without waves, agree with Coles's data. The best way to do this is to convert u_* to a drag coefficient, $C_f = 2u_*^2/U_\infty^2$, and then plot C_f *vs.* R_θ. This plot can be compared with the values of C_f *vs.* R_θ in Coles's table 1. The comparison (figure 3) shows excellent agreement between our data and Coles's data.

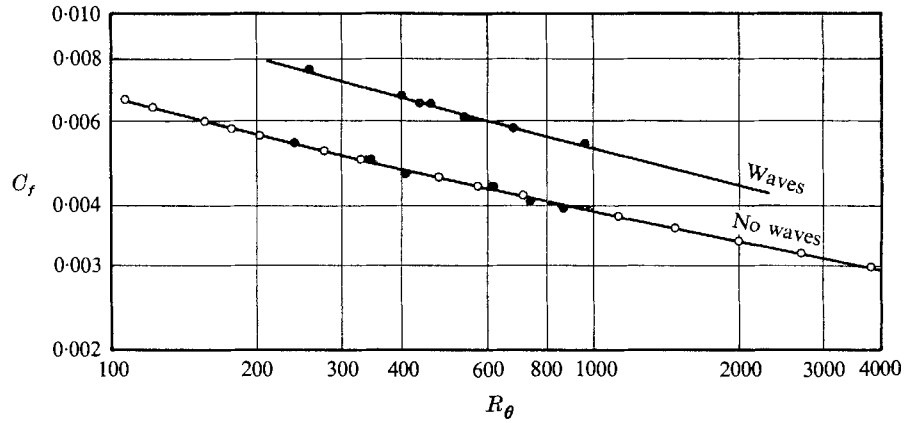

FIGURE 3. Drag coefficient *vs.* momentum Reynolds number of boundary layer. ○, Coles (1954); ●, this study.

The above discussion demonstrates that the mean-velocity profile, in the absence of waves, is quantitatively similar to that over a smooth flat plate if we include the effects of a surface current. The comparison of the profile over waves to previous work is more difficult, because no measurements have been reported for the flow régime considered here, a boundary layer over a small, smooth, sinusoidal wave for wind speeds near the wave phase velocity. Shemdin (1967) reported that mean-velocity profiles above 0·4 Hz waves (wavelength of about 1000 cm) were nearly logarithmic but showed systematic deviations from a least-squares logarithmic fit, contrary to what we find for 40 cm wavelength waves. Hidy & Plate (1966) observed a logarithmic profile over small wind generated waves for wind speeds large compared with the wave speed. Wu (1968) has extended the work of Hidy & Plate and presents very complete measurements of the mean-velocity profile above such waves for large wind speeds. He shows conclusively that, for these high wind speeds, the profile is logarithmic near the water surface and, consequently, the same as the profile over a rough flat plate. Since our profiles are of the same form as those described in the last two papers, although for a different range of parameters, we conclude that the velocity profile over water waves is quantitatively similar to the profile over a rough plate.

5. The wave-induced perturbation velocity field

In the usual development of the linear theory for shearing flow over waves, the velocity field is decomposed by means of the y average as defined by Phillips (1966, page 90); however, in practice, it is more convenient to accomplish the decomposition through a Fourier analysis of the velocity, recorded as a function of time, by an anemometer at a fixed x in the tunnel. To understand how this decomposition is accomplished, consider the spectral forms of the water-surface elevation and air velocity. (Here we use spectra to simplify the discussion. In actuality, the data was analyzed in terms of its Fourier amplitudes.)

The generated wave was very closely sinusoidal and had no ripples on it; so, in a fixed reference frame, the water-surface elevation is

$$z = a\cos(kx - 2\pi f_1 t), \tag{5.1}$$

where k is the wave-number, and f_1 is the wave frequency in Hz. The spectrum of the water-surface elevation, $S_w(f)$, measured at any x, is a line spectrum

$$S_w(f) = \tfrac{1}{2}a^2\delta(f - f_1), \tag{5.2}$$

where δ is the Kronecker delta function. The spectrum of each part of the velocity field, as measured at a fixed x, is as follows: $U(z)$ is constant, and need not concern us here. The ith component of the wave-induced perturbation velocity in the air, $\mathscr{U}_i$, is, by definition, constant at any particular phase of the wave; thus, it repeats itself at the wave frequency, and is of the form

$$\mathscr{U}_i = \mathscr{U}'_i\cos(2\pi f_1 t + \phi_{u_i}), \tag{5.3}$$

where $\{\phi_{u_i}\} = \{\phi_u, \phi_w\}$ is the phase of $\mathscr{U}_i$ with respect to the wave crest; and its spectrum is

$$S_{\mathscr{U}_i}(f) = \tfrac{1}{2}\mathscr{U}'^2_i\delta(f - f_1). \tag{5.4}$$

In (5.3) we have ignored the higher harmonics of the velocity field, mainly because the linear theory predicts only the fluctuations at the wave frequency, and because the principal contribution to the fluctuations comes at the wave frequency. The turbulent velocities, $\{u'_i\}$, have a continuous spectrum, $S_{u'_i}(f)$. Thus the spectrum of the air velocity, $S_{u_i}(f)$, is composed of a continuous spectrum with a superimposed line spectrum.

To separate this line from the background due to u'_i the data should be spectrally analyzed at the narrowest possible bandwidth. For, if one of the frequency bands of the analysis contains f_1, the contribution to the velocity spectrum from this band will be composed of a contribution from $\mathscr{U}_i$ plus a contribution from u'_i.

$$S_{u_i}(f_1) = S_{\mathscr{U}_i}(f_1) + S_{u'_i}(f_1)$$

and, as the bandwidth of the analysis shrinks, $S_{u'_i}$ becomes small, but $S_{\mathscr{U}_i}$ remains constant.

The analysis of noisy periodic signals has been considered by many workers, and the problem is well understood; an example of the analysis used in a problem similar to ours is contained in Munk & Cartwright (1966). We present here only an outline of the analysis with some comments on certain aspects of the problem. Complete details are given in Stewart (1969). For this study, we are interested in

the amplitude and phase of a single sinusoidal component (at the wave frequency); therefore, it is convenient first to calculate the coefficients of the Fourier series expansion of the raw data at the frequencies near the wave frequency, convert these coefficients to those for the Fourier series expansion of velocity and water-surface elevation (assuming a linear instrumental response function), and, finally, to compute the desired spectral and phase relations.

The coefficients of the Fourier series expansion of a series of data samples, $x_k(t\Delta) = x_k(t)$, $t = 1, 2, \ldots, m$; for the kth instrument, is given by

$$X_k(j) = \frac{2}{m} \sum_{t=1}^{m} x_k(t) \exp\left[-i2\pi j(t-1)/m\right] \quad (0 \leqslant j \leqslant \tfrac{1}{2}m), \tag{5.5}$$

where $i = \sqrt{-1}$, $m = 4096$ and Δ, the time interval between samples, is 0·048 sec. To reduce the amount of computation, $X_k(j)$ was only calculated for 20 values of j near the wave frequency. The $X_k(j)$ were manipulated in an obvious way to obtain the coefficients of the Fourier series expansions of the velocity and water-surface elevation. The spectra, $S_k(j)$, cross-spectra, $C_{kl}(j) + iQ_{kl}(j)$, and phases $\phi_{kl}(j)$, were computed using the relations

$$\left.\begin{aligned} S_k(j) &= \tfrac{1}{2}X_k(j)X_k^*(j), \\ C_{kl}(j) + iQ_{kl}(j) &= \tfrac{1}{2}X_k(j)X_l^*(j), \\ \phi_{kl}(j) &= \arctan\left[Q_{kl}(j)/C_{kl}(j)\right]. \end{aligned}\right\} \tag{5.6}$$

Here $X^*(j)$ is the complex conjugate of $X(j)$. A typical example of the velocity and wave spectra, at f near f_1, is given in figure 4. The peak in S_{u_i} in the neighbourhood of f_1, was associated with $S_{\mathscr{U}_i}$. The values of $S_{\mathscr{U}_i}$ and S_w were used to calculate $\mathscr{U}_i'$ and a using (5.2) and (5.4). Note, these latter variables are non-dimensional; to obtain their dimensional values, multiply a by (ν/u_*) and $\mathscr{U}_i'$ by $(a'u_*^2/\nu)$, where a' is $a\nu/u_*$. To be more specific, since $a' = 0{\cdot}64$ cm and $\nu = 0{\cdot}158$ cm^2/sec, the dimensional value of $\mathscr{U}_i$ is computed by multiplying $\mathscr{U}_i'$ by $(4{\cdot}05\,u_*^2)$ cgs.

Throughout these computations, considerable care was taken to avoid numerical errors; and, where possible, the calculations were hand checked. The Fourier analysis was verified by analyzing computer-generated sinusoidal signals; and the entire data collecting system was tested by digitizing and analyzing a sinusoidal electrical signal applied simultaneously to all three data channels in place of the instrumental signals. The phases obtained by the digital analysis were within 1° of being identical, and the amplitudes were within 1 % of a voltmeter measurement of this sinusoidal input signal. Furthermore, the wave height, as deduced from its spectra, agreed with the height as measured by a simple wave staff. The linear analysis was verified by analyzing a portion of data using the exact, non-linear response function of the anemometers. This not only confirmed the validity of the linear approximation, but also provided an independent check of the algorithms used in the linear analysis.

The peak in the various spectra was not always a line, but was usually spread over several elementary frequency bands, as can be seen in the spectrum of the water surface elevation in figure 4. The nature of this spreading depends on the exact frequency of f_1, and the length of record being analyzed; the latter determines the width of the elementary frequency band, while the form determines the

number of bands over which the spreading occurs. It can be shown that if the Fourier analysis is done at frequencies $f = jf_0$, where f_0 is the reciprocal record length, and j any integer; and if $f_1 = gf_0$, g being any real number, then

$$S(j) = \tfrac{1}{2}a^2 \operatorname{sinc}^2(j-g), \tag{5.7}$$

where $\operatorname{sinc} x = (\sin \pi x)/(\pi x)$. Thus, if g is an integer, there is no spreading; and if g falls halfway between values of j, there is maximum spreading. Nevertheless, even in the worst case 90 % of the line spectrum is still contained in the two elementary frequency bands on either side of f_1. Because f_1 varied slowly (at the rate of about 2×10^{-3}Hz/h), it was impossible to adjust f_1 so g was approximately

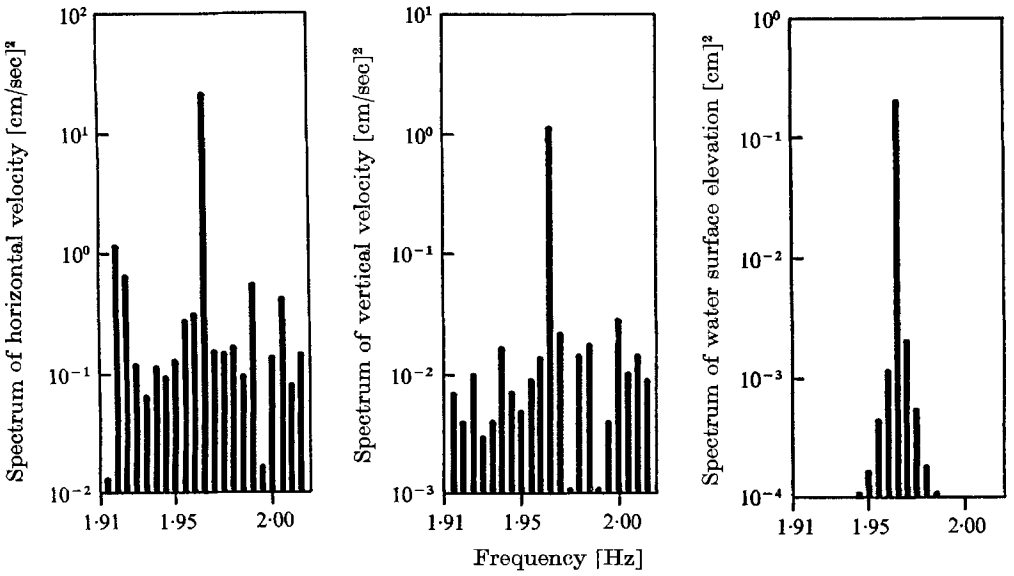

FIGURE 4. Typical spectra of horizontal and vertical air velocities and water-surface elevation at frequencies near the wave frequency.

integer valued, since data were collected over a period of several hours. However, during the time one series of data samples was collected, the frequency did not change enough to broaden the spectral peak. Instead, the only manifestation of this drift was a slow change of the position of the peak with time.

Before comparing the data with theory, consider the accuracy of the data. The measurements of $S_{\mathscr{U}_i}$ are imprecise because they include contributions from $S_{u_i'}$ and because fluctuations in U_∞ cause changes in $U(z)$ and thus ultimately in $S_{\mathscr{U}_i}$. If we define a signal-to-noise ratio

$$SN_{u_i} = \frac{S_{\mathscr{U}_i}}{S_{u_i'}}$$

and estimate the value of $S_{u_i'}$ from its value at neighbouring frequency bands, then we find $SN_{u_i} > 20$ and often > 100. Under these conditions $S_{u_i'}$ contributes little error to the measurements of $S_{\mathscr{U}_i}$. To estimate the effect of slight fluctuations in U_∞ on the measurement of $S_{\mathscr{U}_i}$, some measurements were repeated on the same night and on different nights. In general, the variance in the measured values of

$\mathscr{U}_i'$ was about 20 % of their mean; and the variance in ϕ_{u_i} was about 10°. Thus the imprecision of the measurements was considerably larger than the inaccuracy of each measurement. One entire profile was measured twice and the results of both measurements have been plotted together in figure 6 so one can judge the repeatability of the measurements.

These estimates of accuracy do not apply to the measurements of $\mathscr{W}$ near the region where the mean velocity equals the wave phase velocity. Here the signal-to-noise ratio for $\mathscr{W}$ becomes small, because $\mathscr{W}$ becomes small; and the measurements are inaccurate. However, this loss of accuracy was seldom a problem since this region was narrow.

6. The linear theory

Outline of the theory

The linear theory, used to predict the wave-induced perturbation velocities, $\{\mathscr{U}_i\}$, has been considered by a number of authors. Miles (1957) was the first to formulate the problem so as to obtain solutions useful in practice. Later, the theory was extended by Miles (1959) and Benjamin (1959). Very recently, the problem has been re-examined by Reynolds (private communication) at Stanford and by Davis (1970). These various formulations of the linear theory differ in two respects: (1) Miles's (1957) formulation applies to flows in the limit of infinite Reynolds number, while the other formulations apply to flows of any Reynolds number. (2) Most importantly, each formulation requires an assumption, or hypothesis, about the effects of turbulence in the perturbation equations. Miles assumed that the turbulent Reynold stresses are the same in the perturbed flow as they were in the original flow. This hypothesis results in the so called 'quasi-laminar model', but for our discussion we will call it hypothesis A. Benjamin ignored the effect of turbulent fluctuations, and, consequently, his formulation applies rigorously only to laminar flows. Davis, motivated by Benjamin, reformulated the theory to include the effects of turbulence, and considered two different models. The first used hypothesis A, and is the same as Miles's formulation except for the inclusion of viscous terms. The second model assumed that turbulent Reynolds stresses are a function of an appropriate measure of the elevation above the instantaneous water surface. We designate this hypothesis B. Reynolds assumed the turbulent Reynolds stresses could be related to the mean flow by a constitutive equation which is equivalent to introducing an eddy viscosity.

Miles was able to obtain approximate solutions to his perturbation equation by means of asymptotic expansions, for a velocity profile of the form $U = U_1 \ln(z/z_0)$. The expansion required (i) that viscous effects be important only near the wall and near the critical layer, z_c, where the mean-wind velocity equals the wave phase velocity; and (ii) that these two regions be well separated. For the lower wind speeds the viscous layer about the critical layer is wider than that near the wall and (ii) requires, in effect, that

$$z_c \gg \left[\frac{\nu}{U_c' k}\right]^{\frac{1}{3}}, \tag{6.1}$$

where U_c' is the derivative of U evaluated at the critical layer. For this condition to apply to the experimental flow, $z_c \gg 0{\cdot}6$ cm, a condition apparently met for one set of data, when $z_c \simeq 4$ cm. If the conditions for the asymptotic theory are met, the wave-induced Reynolds stress should be

$$\rho\overline{\mathscr{U}\mathscr{W}} = 0 \quad (z > z_c),$$

$$= -\frac{\pi}{k}\frac{U_c''}{U_c'}\overline{\mathscr{W}_c^2} \quad (z < z_c), \tag{6.2}$$

i.e. the Reynolds stress should have a step discontinuity at the critical layer. This immediately suggests that one should measure $\rho\overline{\mathscr{U}\mathscr{W}}$ as a function of height for those mean-velocity profiles which enable one to measure below the critical layer. This should yield a region near the surface where $\rho\overline{\mathscr{U}\mathscr{W}}$ is constant and negative, thus it can be extrapolated to just outside the viscous surface layer to obtain the momentum transfer to the wave due to the wave-induced perturbation velocities. This was initially the purpose of the experiment.

The complexity of the perturbation equations formulated by Davis and by Reynolds makes it impossible to obtain even approximate analytic solutions; but they are amenable to solution by numerical methods for the range of parameters investigated in the experiment. Both Davis and Reynolds integrated numerically their perturbation equations to obtain profiles of $\mathscr{U}_1$, ϕ_{u_i}, and $\rho\overline{\mathscr{U}\mathscr{W}}$ that were directly comparable with the data; and we are thankful to them for this material. The shape of these profiles was unexpected in one respect, the wave-induced Reynolds stresses were not constant in the region $z < z_c$ where the asymptotic theory predicted they would be constant.

This unexpected behaviour of the wave-induced stresses, which is obviously due to the effects of viscosity, was first noted by Reynolds. Davis investigated the effects of viscosity more explicitly, and obtained estimates of the size of the viscous regions. In particular, although (6.1) is valid for each velocity component, the viscous region for the Reynolds stresses is much wider. Furthermore, Davis showed that even when the asymptotic theory should apply, viscosity seriously influences the momentum transfer to the wave, and thus the momentum transfer cannot be estimated accurately from the velocity field measured inside the critical layer but outside the viscous sublayer.

Comparison between theory and measurements

Before proceeding to a comparison of theory to measurement, we must discuss the applicability of the theory to the tunnel conditions. Firstly, $ka = 0{\cdot}10$; so the linear theory, which assumes $ka \ll 1$, should apply. Secondly, $kD = 5{\cdot}7$, where D = height of the top of the tunnel above the water surface; so the top on the tunnel should have little effect on the flow near the waves. More importantly, the theoretical airflow was assumed to have no x or y gradients, while the tunnel flow had variations of ± 5 % in the y, z plane (perpendicular to the tunnel axis), excluding boundary layers; and the flow in the boundary layers was developing in the downstream direction. The effect of the former variation is not precisely known, but its effect can be estimated by determining whether the measured flow

obeys continuity in two dimensions. This is done later in this section. The change in u_* in the downstream direction, in the boundary layer over the waves, although difficult to measure accurately, was about 5–10 %/wavelength at the point where the perturbation velocities were measured. This change in u_* appears to be small, but its effect is unknown. Furthermore, because of the shortness of the tunnel, meaningful measurements of this effect could not be made.

The numerical integrations available for comparison with the data were quite extensive. Reynolds integrated his perturbation equation for three of the profiles

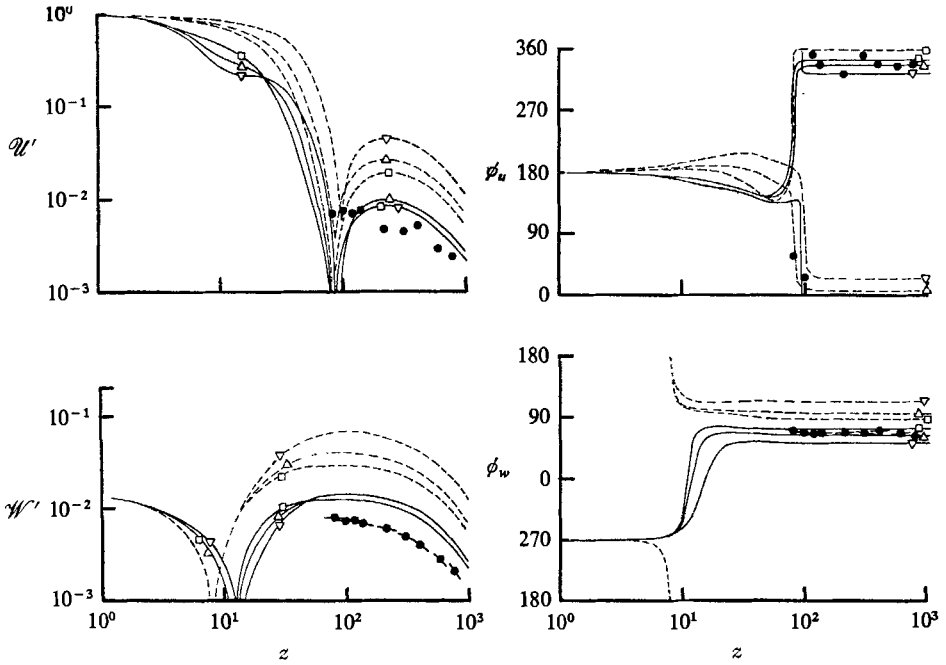

FIGURE 5. Wave-induced perturbation velocity *vs.* height for $U_\infty = 277$ cm/sec. – – –, integrations of equation associated with hypothesis A; —, with hypothesis B; △, with $u_* = 1{\cdot}05\,u_*$ in table 1, using profiles $\delta = 10$, $\gamma = 3{\cdot}3$; ▽, $\delta = 15$, $\gamma = 3{\cdot}51$; □, $\delta = 7$, $\gamma = 2{\cdot}3$. ○, with $u_* = u_*$ in table 1, using profile $\delta = 10$, $\gamma = 3{\cdot}3$. ●, data. Lines through $\mathscr{W}$ data calculated from $\mathscr{U}$ data assuming continuity.

investigated by the experiment; while Davis integrated his equations for all profiles, and, in addition, investigated the effect or errors in various experimental parameters. Because of the large number of integrations calculated by Davis, we confine our attention primarily to his results.

The profiles used in his integrations were calculated from (4.2), and are identical to those in figure 2. These different profiles were used to investigate the consequences of a lack of knowledge of U in the region where measurements could not be made. The data for the wave-induced velocity field, together with representative numerical integrations, are given in figures 5–11. The integrations shown give the most distinctive or the most different velocity fields and not necessarily the best fit with the data. In general, the integrations not shown fell between those that were. The slopes drawn through the $\mathscr{W}'$ and ϕ_w data were

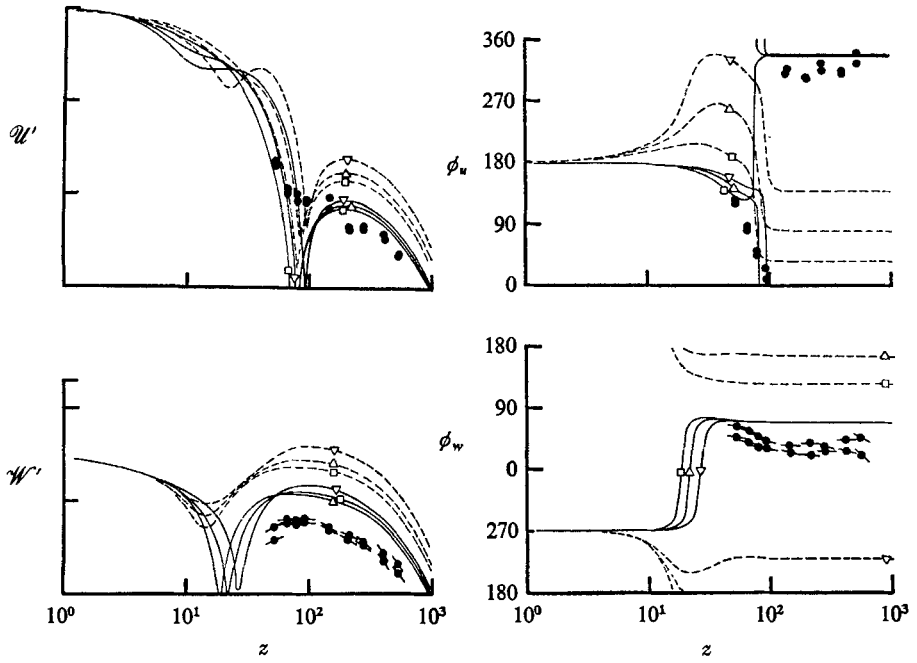

FIGURE 6. Same as figure 5 except $U_\infty = 155$ cm/sec.

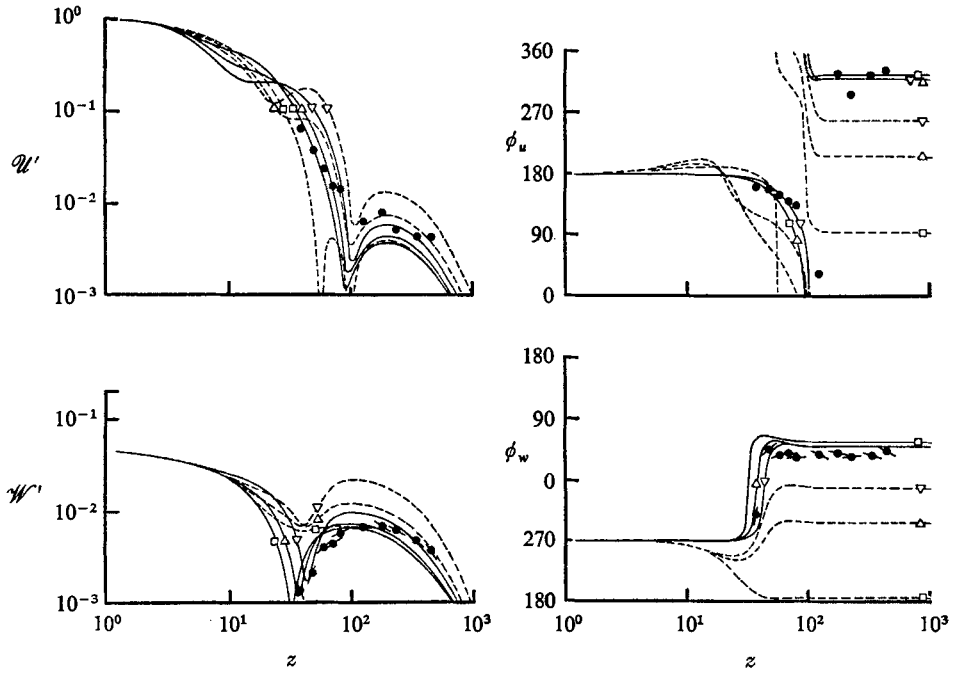

FIGURE 7. Same as figure 5 except $U_\infty = 120$ cm/sec.

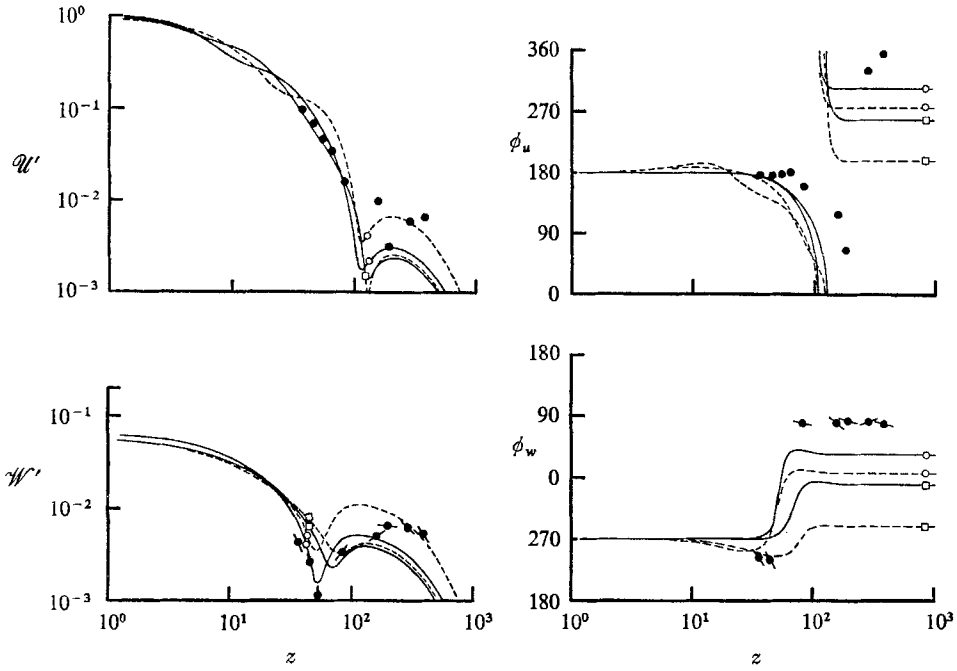

FIGURE 8. Same as figure 5 except $U_\infty = 102$ cm/sec.

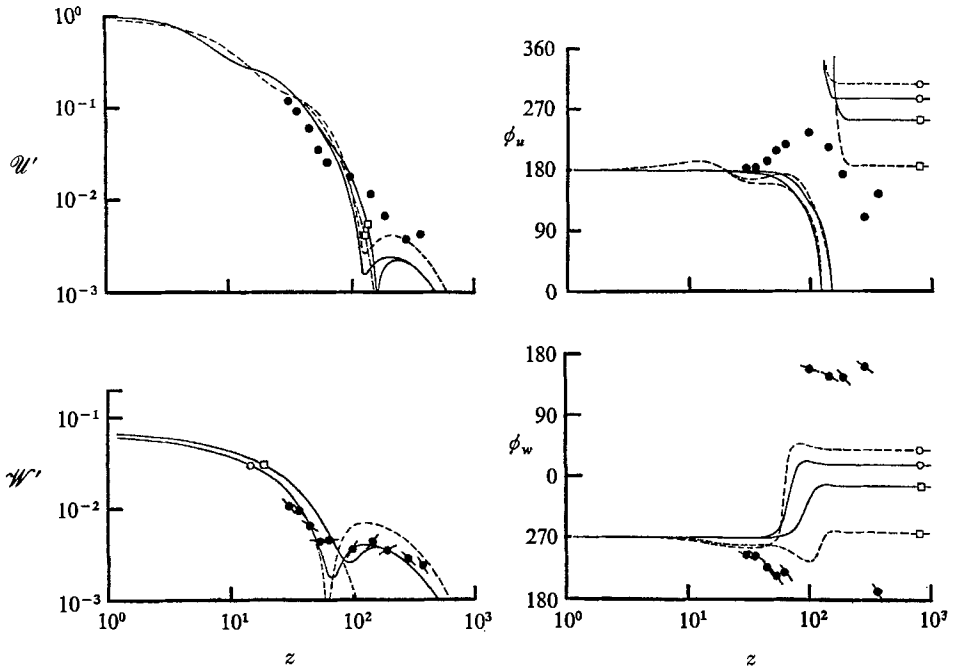

FIGURE 9. Same as figure 5 except $U_\infty = 95$ cm/sec.

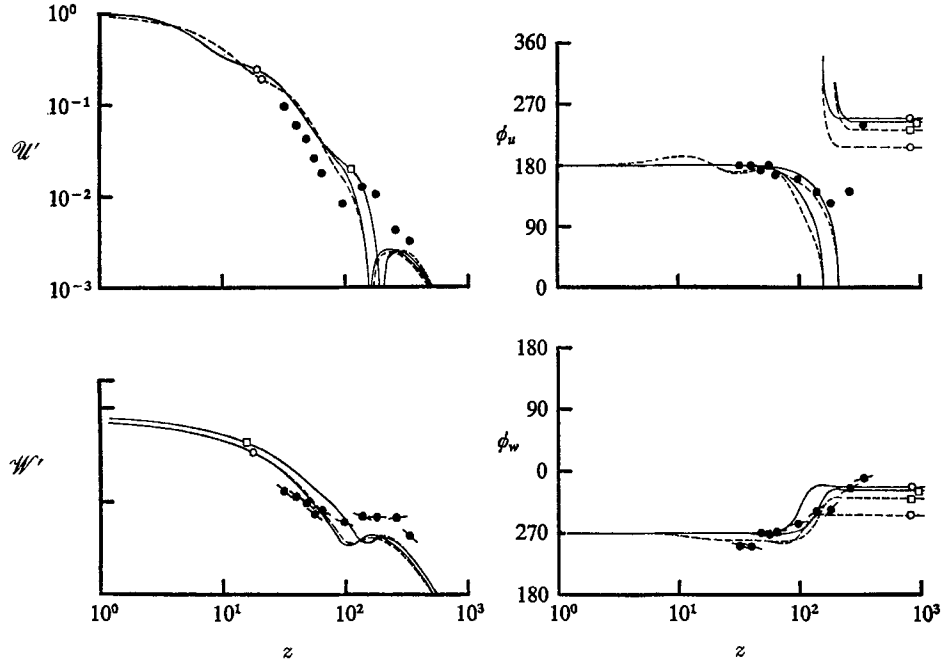

FIGURE 10. Same as figure 5 except $U_\infty = 86$ cm/sec.

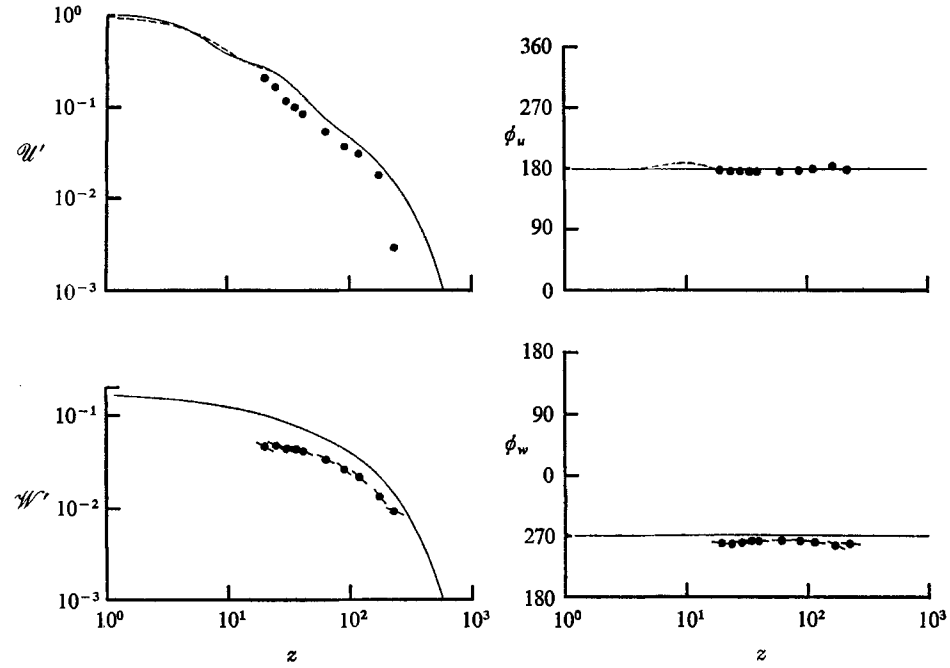

FIGURE 11. Same as figure 5 except $U_\infty = 56$ cm/sec.

calculated from the $\mathscr{U}$ data assuming continuity in two dimensions. This can be done accurately since

$$\frac{\partial \mathscr{U}}{\partial x} + \frac{\partial \mathscr{W}}{\partial z} = 0 \tag{6.3}$$

and since, from (5.3), for any x, $\mathscr{U} = \mathscr{U}' \cos(kx - 2\pi f_1 t - \phi_u)$; thus $\mathscr{U}$ can be differentiated explicitly to obtain the desired z derivatives. This provides a check on whether the data obey continuity in the x, z plane; if the data points do not follow the calculated derivatives, then the data may be in error, or the flow may have important three-dimensional components and cannot be considered to be two-dimensional. Fortunately, the data points do tend to follow the indicated slopes, although with some scatter.

The figures indicate there is only rough agreement between the measured amplitudes, $\mathscr{U}'_i$, and the amplitudes of the numerical integrations of the equation resulting from hypothesis B, and that the integrations tend to be slightly larger than the $\mathscr{W}'$ data at the higher wind speeds. Nevertheless, there exists one region in each figure where the data does not agree with the integrations, the $\mathscr{U}'$ data does not become small in the region where the integrations go to zero. This is not altogether unexpected since this region is very narrow, and any unsteadiness in the mean flow would tend to smear out this feature, resulting in increased variability in $\mathscr{U}'$. And, indeed, this increased variability was observed; the $\mathscr{U}'$ data tended to be much more variable than the $\mathscr{W}'$ data. The comparison of the phase data with the integrations again shows only rough agreement; in some figures the agreement is very good, but in one it is poor.

A comparison of the data with the integrations of the equation resulting from hypothesis A shows little agreement. The amplitudes tend to be too high at the higher wind speeds, and the phases show poor agreement.

For brevity, Reynolds's solutions have not been presented. His integrations of the equations resulting from the inclusion of an eddy viscosity in the linear theory are of very similar shape and have almost the same amplitudes as the integrations associated with hypothesis A. The phases of his velocities show slightly better agreement with the data than do the phases for the velocities calculated assuming hypothesis B.

In the preceding paragraphs we have compared the measured velocity fields to those predicted by three different linear theories based on three different arbitrary assumptions concerning the role of turbulence in the linear theory. This comparison showed that none of the three theories can predict the velocity field well. The instability theories can give the correct qualitative nature of the velocity field, but not its quantitative value.

Up to this point we have not considered the wave-induced Reynolds stresses because of the special difficulties involved in their measurement. The nature of these difficulties can best be explained by considering three features of the theoretical velocity fields. Firstly, $\mathscr{U}$ and $\mathscr{W}$ were almost exactly in quadrature; they rarely deviated more than 10° from being 90° out of phase. Secondly, $\overline{\mathscr{U}\mathscr{W}}$ was oscillatory in z, with large gradients near the water surface. Thirdly, the calculated Reynolds stresses were more sensitive to variations in U and u_* than were the components of the velocity field. Because the measured Reynolds

stresses are qualitatively similar to the calculated stresses, these features of the stresses have the following implications: (1) The close approximation to quadrature between $\mathscr{U}$ and $\mathscr{W}$ implies that small errors in the measurement of their phases will result in large errors in $\overline{\mathscr{U}\mathscr{W}}$. Indeed, this was observed; repeated measurements of $\overline{\mathscr{U}\mathscr{W}}$ differed by up to $\pm 50\,\%$ of their mean. (2) The oscillatory nature of the stresses, with large gradients, implies that the finite size of the velocity probe will distort the measurements to some extent, especially near the water. (3) The sensitivity of the calculated stresses to small perturbations in U and u_* makes comparison between theory and experiment difficult.

Because of these difficulties, no direct comparisons have been made between the measured and calculated stresses. Any agreement between theory and measurement would be due more to chance than necessity. However, certain conclusions can be drawn from the data. The measured wave-induced Reynolds stresses were qualitatively similar to the calculated stresses, and confirmed that viscosity was important for the flow. Furthermore, because these stresses had no constant stress layer, they could not be used to calculate the momentum transfer to the wave.

7. Discussion

In this section, we will make use of the data for the flow over laboratory waves to comment on some previously hypothesized, qualitative aspects of the flow, and on their relationship to recent field measurements.

In the past, there has been some controversy about the shape of the velocity profile above different phases of the wave. Benjamin, on the basis of data from boundary layers above curved surfaces, assumed that the boundary layer over a wave would, to a first approximation, be the same at every point along the wave if it were measured as a function of $\eta = z - ae^{kz}\cos kx$. However, Shemdin (1967) indicated that the mean-velocity profile over the crest differed from that over a trough. To examine the question, we have plotted $(U + a\mathscr{U})u_* vs. (z^+ - \zeta)$, where ζ is the water surface elevation, using their values over a crest ($\zeta = au_*/\nu$) and over a trough ($\zeta = -au_*/\nu$). This is approximately the same as plotting $(U + a\mathscr{U})\,u_* vs. \eta$ since $kz \ll 1$. Furthermore, because of the nature of the logarithmic profile, this approximation introduces still less error into the plot. The result is shown in figure 12. This figure shows that the mean-velocity profile does appear to be the same over the crest and trough if it is plotted relative to the water surface, although there is a systematic discrepancy which increases as the wind speed increases. This discrepancy does not contradict the linear theory, and it is exactly such a discrepancy that must exist if there is to be a transfer of momentum from the air to the wave due to a wave-induced Reynolds stress.

Another source of confusion has been the expected size of the wave-induced Reynolds stress, $\rho\overline{\mathscr{U}\mathscr{W}}$. Stewart (1961) proposed that, over a fully developed sea, a major proportion of the stress at the water surface is carried by $\rho\overline{\mathscr{U}\mathscr{W}}$, and, as a consequence, the boundary layer near the water surface will be strongly organized, and thus considerably different from the turbulent boundary layer over a flat plate. However, Stewart (1967) reported that measurements by Smith showed the wave-induced velocity field to be much smaller than anticipated, and, in fact,

could not be measured. The data presented in this paper suggests an explanation for these negative results.

In reporting Smith's data, Stewart estimated the expected size of the velocity field from Miles' first approximation to the flow, to obtain

$$\left.\begin{aligned} S_{\mathscr{U}} &= \tfrac{1}{2}[ka(U-c)-aU']^2\, e^{-2kz}, \\ S_{\mathscr{W}} &= \tfrac{1}{2}[ka(U-c)]^2\, e^{-2kz}. \end{aligned}\right\} \tag{7.1}$$

We have computed $S_{\mathscr{U}}$, $S_{\mathscr{W}}$ from (7.1) using (4.2) with $C_1 = 3{\cdot}7$, $\delta = 15$, $\gamma = 5$;

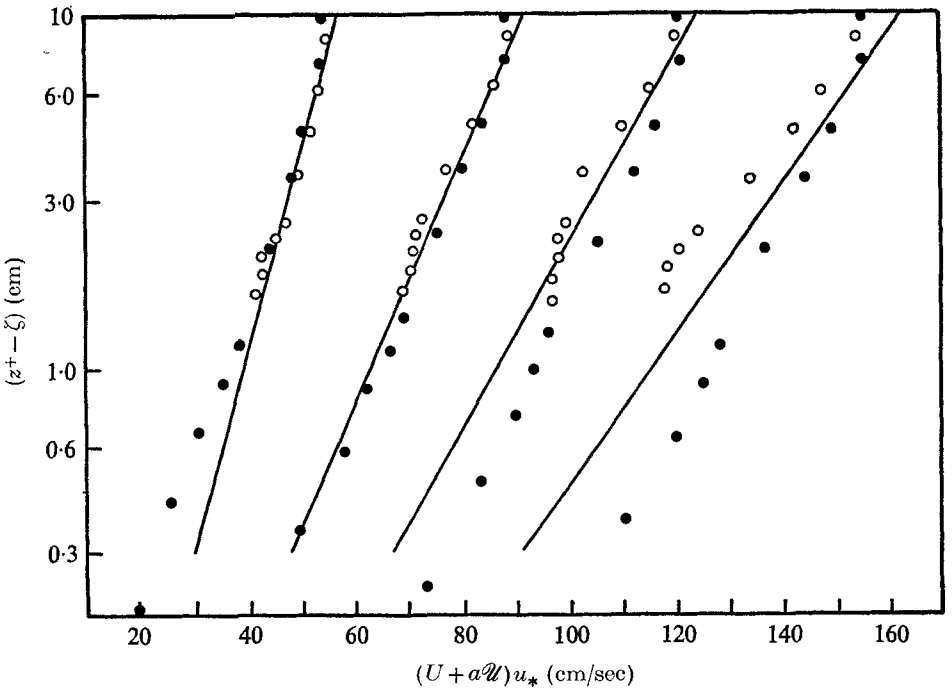

FIGURE 12. Mean-wind velocity as a function of wave phase *vs.* instantaneous height above water surface; ●, over a crest; ○, over a trough.

a comparison of these computed spectra with the measured spectra shows that (7.1) provides a correct estimate of the spectra when $U \simeq c$, but significantly overestimates the spectra, by as much as a factor of four, at both higher and lower wind speeds. The greater or lower the wind speed, the greater the disagreement. This, then, adequately explains the failure of Smith, as reported in Stewart, to see the wave-induced velocity field, for, if it were $\frac{1}{4}$ of its value as estimated by (7.1), it would be barely above the background noise due to the turbulent fluctuations in the boundary layer, for the bandwidth of his analysis, and would go unobserved.

There remains one final comment; the data and the numerical integrations clearly indicate the effects of viscosity are more important than has previously been estimated, and the asymptotic theory for the growth of waves should be applied with caution, especially in laboratory studies where the Reynolds

number of the flow tends to be comparatively low. This effect of viscosity may help explain the discrepancy between the calculated and the measured rate of growth of wind-generated waves in recent experiments.

The author wishes to thank J. W. Miles and R. E. Davis for their advice and comments. This work was supported by the Office of Naval Research under Contract Nonr-2216(29N) and is based on a dissertation (Stewart 1969) submitted to the University of California, San Diego.

REFERENCES

BAINES, W. D. & KNAPP, D. J. 1965 Wind driven water currents. *J. Hydr. Div., Proc. A.S.C.E.* HY2, 205–221.

BARNETT, T. P. & WILKERSON, J. C. 1967 On the generation of ocean wind waves as inferred from airborn radar measurements of fetch-limited spectra. *J. Mar. Res.* **25**, 292–328.

BENJAMIN, T. B. 1959 Shearing flow over a wavy boundary. *J. Fluid Mech.* **6**, 161–205.

BOLE, J. B. & HSU, E. Y. 1969 Response of gravity water waves to wind excitation. *J. Fluid Mech.* **35**, 657–675.

COLES, D. 1954 The problem of the turbulent boundary layer. *Z. angew. Math. Phys.* **5**, 181–203.

DAVIS, R. E. 1970 On the turbulent flow over a wavy boundary. *J. Fluid Mech.* **42**, 721.

HIDY, G. M. & PLATE, E. J. 1966 Wind action on water standing in a laboratory channel. *J. Fluid Mech.* **26**, 651–687.

HINZE, J. O. 1959 *Turbulence.* New York: McGraw-Hill.

KEULEGAN, G. H. 1951 Wind tides in small closed basins. *J. Res. Nat. Bur. Standards*, **46**, 358–381.

MILES, J. W. 1957 On the generation of surface waves by shear flows. *J. Fluid Mech.* **3**, 185–204.

MILES, J. W. 1959 On the generation of surface waves by shear flows. Part 2. *J. Fluid Mech.* **6**, 568–582.

MILES, J. W. 1965 On the generation of surface waves by shear flows. Part 5. *J. Fluid Mech.* **30**, 163–175.

MUNK, W. H. & CARTWRIGHT, D. E. 1966 Tidal spectroscopy and prediction. *Phil. Trans. Roy. Soc.* A **259**, 533–581.

PHILLIPS, O. M. 1966 *The Dynamics of the Upper Ocean.* Cambridge University Press.

ROSHKO, A. 1955 On the development of turbulent wakes from vortex streets. *Nat. Adv. Comm. Aero. Rep.* 1191, Wash. D.C.

SEEHOLTZ, J. R. 1968 A field investigation of air flow immediately above ocean surface waves. *Dept. of Meteorology Rep., Mass. Inst. Tech.*

SHEMDIN, O. H. 1967 Experimental and analytical investigations of the air velocity above progressive waves. *Stanford University. Dept. Civil Engng. Tech. Rep.* 82.

SHEMDIN, O. H. & HSU, E. Y. 1966 The dynamics of wind in the vicinity of progressive water waves. *Stanford University. Dept. Civil Engng. Tech. Rep.* 66.

SHEMDIN, O. H. & HSU, E. Y. 1967 Direct measurements of aerodynamic pressure above a simple progressive gravity wave. *J. Fluid Mech.* **30**, 403–416.

SNYDER, R. L. & COX, C. S. 1966 A field study of the wind generation of ocean waves. *J. Mar. Res.* **24**, 141–178.

STEWART, R. H. 1969 Laboratory studies of the velocity field over deep-water waves. Ph.D. dissertation, University of California, San Diego.

STEWART, R. W. 1961 Wave drag over water. *J. Fluid Mech.* **10**, 189–194.

STEWART, R. W. 1967 Mechanics of the air-sea interface. *Phys. Fluids*, **10**, S47–S55.

TAKEDA, A. 1963 Wind profile above sea waves. *J. oceanographical Soc. Japan* **19**, 136–142.

WEILER, H. S. & BURLING, R. W. 1967 Direct measurements of stress and spectra of turbulence in the boundary layer over the sea. *J. Atmospheric Sci.* **24**, 653–664.

WU, J. 1968 Laboratory studies of wind–wave interactions. *J. Fluid Mech.* **34**, 91–111.